The Hydrophosphination of Styrene and Polymerisation of Vinylpyridine: A Computational Investigation of Calcium Catalysed Reactions and the Role of Fluxional Non-Covalent Interactions.

Bryan J. Ward* and Patricia A. Hunt*

Department of Chemistry, Imperial College London, London, SW7 2AZ, UK.

ABSTRACT: A computational investigation of the intermolecular hydrophosphination of styrene and 2-vinylpyridine, catalysed by the heteroleptic β-diketiminato-stabilised calcium complex [(PhNC(Me)CHC(Me)NPh)CaPPh$_2$], is presented. Alkene insertion does not proceed via the traditional route as proposed by experimental and theoretical research related to intermolecular hydroamination catalysed by alkaline earth or lanthanide complexes. In contrast, for the hydrophosphination mechanism, insertion proceeds via an outer sphere, conjugative addition where there is no direct interaction of Ca with the vinyl functionality. Following the initial rate determining alkene insertion, two distinct mechanisms emerge, protonolysis or polymerisation. Polymerisation of styrene is energetically less favourable than protonolysis whereas the reverse is determined for 2-vinylpyridine, thereby providing strong evidence for outcomes observed experimentally. The vinylarene ring is important as it allows for preferential coordination of the unsaturated substrate through numerous non-covalent Ca···π, CH···π and Ca←E (E=P, N) interactions, moreover the vinylarene ring counteracts unfavourable charge localisation within the activated transition state. The additional stability of the Ca←N over Ca←P dative interaction in vinylpyridine provides a rationalisation for the experimentally observed enhanced reactivity of vinylpyridine, particularly in the context of the almost identical local alkene insertion barriers. Previously, little emphasis has been placed on the involvement of non-covalent interactions however, our calculations reveal that Ca···π, CH···π and Ca←donor interactions are critical; stabilising key intermediates and transition states, while also introducing numerous competitive pathways. KEYWORDS: Alkaline earth metals, calcium, density functional theory (DFT), heterofunctionalisation, hydrophosphination, non-covalent interactions, polymerisation, protonolysis.

INTRODUCTION

Hydrophosphination (describing the addition of H–P over unsaturated C–C or C–X (X = O, N, S) bonds) is a relatively understudied heterofunctionalisation reaction compared to hydroamination processes, yet this reactivity is an atom-efficient route to organophosphines. Organophosphines are ubiquitous with transition metal chemistry and have a prominent role in homogenous and asymmetric catalysis as well as in medicinal chemistry.[1-3,4] Moreover, organophosphines are also of significant interest as derivatives to phosphonium-based ionic liquids (ILs). Phosphonium ILs exhibit higher thermal stabilities and conductivities when compared to their corresponding ammonium IL counterparts,[5-10] are an attractive alternative class of solvents to more traditional volatile organic compounds,[11,12] can be used for gas capture[13] and demonstrate antimicrobial properties.[14,15]

Experimentally, there are a number of Ca-based complexes that have been shown to catalyse the hydrophosphination reaction.[16-19] Unlike transition metal catalysts, Ca (and heavier alkaline earth (Ae)) cationic (2+) complexes consist of an electron deficient (d^0) metal centre. Unwanted oxidation/reduction pathways typically associated with transition metals can be avoided as the metal oxidation state remains unperturbed during the reaction. Thus researchers are actively pursuing Ca catalysts as potential alternatives to expensive, toxic, rare metal complexes.[20]

One of the earliest examples of a Ca-complex used to catalyse the hydrophosphination of vinylarenes was the heteroleptic β-diketiminato-stabilised calcium complex [ArNC(Me)CHC(Me)NAr)Ca(NSiMe$_3$)$_2$](Ar=2,6-diisopropylphenyl) (denoted as **E1** in Scheme 1) demonstrated by the Hill group.[16] A range of alternative Ca-based complexes demonstrating catalytic activity in the hydrophosphination reaction have also been identified.[17,21,22]

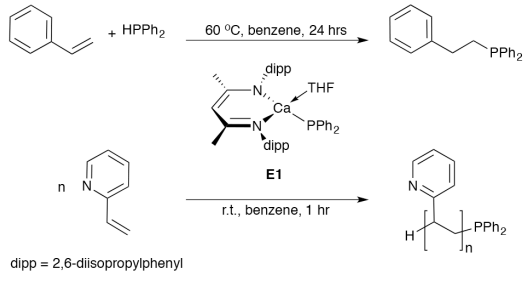

Scheme 1. Active calcium catalyst (E1) employed for the hydrophosphination of styrene and polymerisation of vinylpyridine.

As experimental interest in the Ca-catalysed hydrophosphination reaction continues to intensify, certain aspects of the reaction mechanism remain poorly understood. This includes, the stabilising effect of the Ae-bound ancillary ligands, the impact of

the ancillary ligands on reactivity and the effect of activated vinylarenes.[16-19,23] All of which are addressed within this article.

In this study we investigate, using DFT calculations, main group catalysed C–P bond formation. Crucially, we provide a deeper level of understanding for each of the steps involved in the reaction pathways. While a number of DFT studies complementing experimental research related to Ae-catalysed hydroamination reactions have been conducted,[24-27] to the best of our knowledge, this is the first example of a theoretical evaluation of Ae-catalysed hydrophosphination of vinylarenes.

The Ca-catalysed hydrophosphination reaction is highly dependent on the nature of the unsaturated substrate.[16,17,22,23] When 2-vinylpyridine (referred to as vinylpyridine in the following) was used in place of styrene, the reaction did not undergo hydrophosphination. Instead, the formation of phosphine-capped poly(vinylpyridine) was observed at a much lower temperature and reduced reaction time. Researchers attributed the difference in reaction outcome to a competition between alkene insertion into the Ca–C bond and the first σ-bond metathesis step in the catalytic cycle.[16] In view of the divergent mechanisms reported by the Hill group we evaluate the rival mechanisms for styrene and vinylpyridine.

A key aspect of this work is to characterise and better understand the diverse interactions of large electron rich, sterically bulky ligands from a computational perspective. We examine the range of non-covalent interactions between catalyst and substrate that are critical to understanding the mechanism. The influence of the aryl rings (Ph in styrene and pyridine in vinylpyridine) on the insertion mechanism are examined by comparison with ethene insertion. Our analysis shows that these are essential to understanding the mechanism for Ae systems, which (experimentally) require large kinetically stabilising ancillary ligands. Such an analysis has only recently become possible due to improvements in computational resources, advances in modern codes (improving the speed of computation) and crucially, the incorporation of dispersion corrections to DFT methodologies.

The results and discussion will proceed as follows. First the specific catalyst and reactants computationally modelled will be discussed. The general catalytic cycle will be introduced, highlighting the relative energy of key intermediates and transition states. This will be followed by a detailed examination of the fluxional bonding interactions, which play a significant role in the individual steps of the catalytic cycles for both styrene and vinylpyridine.

RESULTS AND DISCUSSION

Computational Model. In brief, we employ ωB97X-D in association with a Stuttgart/Dresden ECP and associated basis set for Ca, a 6-31G(d,p) basis set for H and C and 6-311G(d,p) basis set for P and N. A conductor-like polarisable continuum model was applied with benzene as the solvent. Natural Bond Orbital analysis was carried out using NBO 5.9.[28] The topology of the electron density for selected systems within the QTAIM framework was carried out using the AIMALL software.[29] Full details of the computational method are presented in the ESI. This method and basis set was chosen to allow accurate calculations to be performed on our largest systems (114 atoms and 450 electrons) within a timely manner.

Ae···π, Ae···H–X and CH···π interactions are dispersion dominated and can have a significant influence on structural organisation. Dispersion corrections are recovered by modern computational methods however, dispersion corrected functionals are also known to overestimate weak interactions.[29-31] Therefore it is important that a suitable functional is selected. Previous theoretical investigations have demonstrated the good performance and recovery of dispersion interactions involved in hydroamination catalysis using B97-D.[24,27] Improved performance has been observed using ωB97X-D, in particular, the evaluation of geometries, thermochemistry and recovery of long-range dispersion interactions.[32-37]

Experimentally, the active catalyst was identified as the β-diketiminate-stabilised calcium complex (**E1,** Scheme 1). The presence of a sterically demanding spectator ligand helps to stabilise the Ae metal centre against lability and brings to the fore the importance of Ae···π, Ae···H–X and CH···π interactions.[16,38,39,40-42] Such interactions have previously been overlooked due to difficulties in synthetic procedures as a consequence of high reactivity.[43] As a corollary, these interactions have also been largely ignored computationally. The size and configurational complexity of the stabilising ancillary ligands in the Ae-metal catalysts has usually lead to over simplified models being employed, while attention is focused on the catalytically active metal and substrate. We retain the β-diketiminate ligand, however to reduce the computational cost, structural simplifications have been required. The phenyl rings are explicitly modelled, however the isopropyl groups have been replaced with H atoms to maintain steric bulk while avoiding the conformational issues associated with the multiple orientations of the isopropyl substituents. This model ligand is subsequently referred to as BDI.

The co-ligand THF has also been removed from the computational model. THF is present in the crystal structure of **E1**, and is likely a contaminant left over from the synthesis of the calcium complex. ^{1}H NMR studies conducted on a similar calcium catalyst indicate that THF dissociates from the complex under catalytic conditions.[17] Recent computational studies by Tobisch, exploring the intermolecular hydroamination reaction at a barium complex demonstrated that THF does not play a direct role in the catalytic cycle. The presence of THF stabilises the catalyst and calculations suggest that THF exists in an association/dissociation equilibrium when amine reactant and product substrates are employed.[24] Preliminary calculations comparing the relative energies associated with the coordination of various reaction substrates at the active Ca catalyst also support this hypothesis (ESI, Table S1).

There are inherent difficulties in calculating accurate Gibbs free energies, which are well documented.[44-46] Large structures such as the bulky spectator ligands, as well as methyl-containing substituent groups, can result in low frequency modes due to small internal rotations. These soft rotations are approximated as simple harmonic vibrations, which can introduce significant errors particularly when calculating entropy.[46] Dispersion and solvent models can have a strong influence on low frequency modes and increase their occurrence. In particular, translation and rotation motions of a molecular system, which contribute significantly to entropy are hindered in solution.[44,46,48,49] Consequently, solvent corrected entropy and subsequently Gibbs free energy of a system in solution can be overestimated. Therefore, enthalpies, as well as

Gibbs free energies are often employed for comparison, and we report both throughout this article.

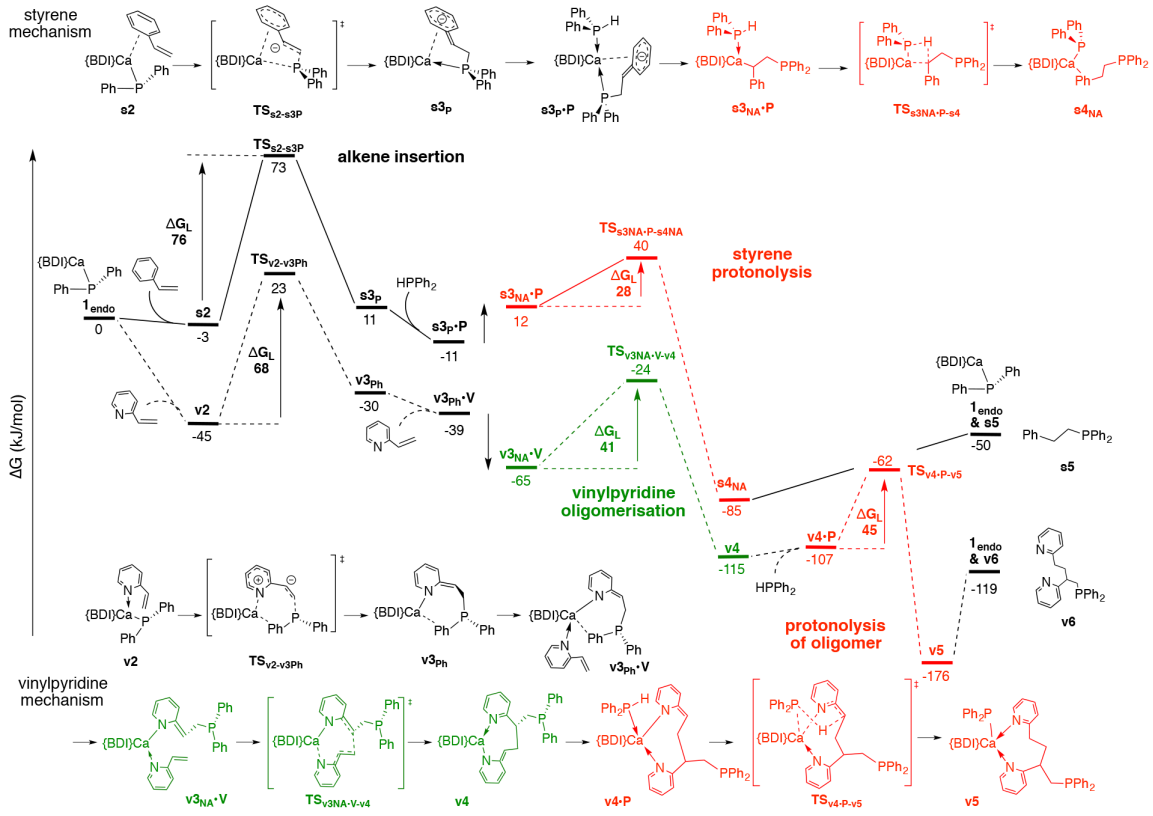

Figure 1. The relative Gibbs free energy profile for styrene hydrophosphination (solid line) and vinylpyridine oligomerisation (dashed line) mechanisms. Alkene insertion in black, protonolysis in red and polymerisation in green. All energies are ΔG_G in kJ/mol.

General Catalytic Cycle. Figure 1 outlines the general Gibbs free energy profile as well as the intermediates and transition states involved in the transformation of styrene (designated s) and vinylpyridine (designated v). Thermodynamic quantities (X= G, H or S) can be global, relative to the starting materials ΔX_G, or local, relative to the "reactants" of the previous step in the mechanistic cycle, ΔX_L. A breakdown of ΔG in terms of ΔH and TΔS (T= 298.15K) are presented in ESI Table S2 and Table S3 respectively.

Both mechanisms start similarly, coordination of styrene or vinylpyridine substrates at the active catalyst, **1**$_{endo}$, giving the alkene activation precursor intermediates **s2** and **v2** respectively. The Gibbs free energy of formation of **s2** (ΔG_G = -3 kJ/mol) lies within the error of the computational method indicating facile styrene coordination whereas the formation of **v2** (ΔG_G = -45 kJ/mol) is favourable relative to the separated alkene and active catalyst constituents.

Surprisingly, alkene insertion does not proceed via the traditional alkene insertion step as proposed by previous experimental and theoretical research related to intermolecular hydroamination catalysed by Ae or La complexes.[24,50] In contrast, we found that alkene insertion proceeds via a conjugative addition mechanism, which is comparable to the transition state involved in the hydrophosphination of 1,3-butadiene.[51] The alkene insertion transition state structures, **TS**$_{s2\text{-}s3P}$ and **TS**$_{v2\text{-}v3Ph}$, will be explored in greater detail in a later section. Nevertheless, the local energy barriers (ΔG_L) associated with alkene insertion (76 kJ/mol for styrene and 68 kJ/mol for vinylpyridine) correspond to the rate-limiting step for both pathways, concurrent with experimental observation.[16,52]

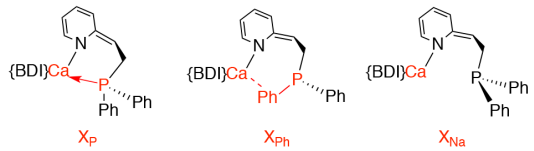

Figure 2. Representative diagrams of the three different coordination modes, X is the structure identifier.

Decay from **TS**$_{s2\text{-}s3P}$ or **TS**$_{v2\text{-}v3Ph}$ leads to the intermediates **s3**$_P$ and **v3**$_{Ph}$, both of which exhibit important stabilising interactions. In the following, labels with a subscript "P" will refer to the dative Ca←P interaction, those with a subscript "Ph" will refer to a Ca···π interaction involving a phenyl ring at P and the subscript "NA" will refer to a lack of stabilising interactions (Figure 2). Therefore, in **s3**$_P$ a dative Ca←P interaction is prevalent whereas in **v3**$_{Ph}$ a Ca···π interaction exists between Ca and a phenyl ring of the phosphine moiety.

From this point the two mechanisms diverge. Continuation of the styrene hydrophosphination mechanism proceeds upon the favourable coordination of diphenylphosphine ($HPPh_2$) at **s3**$_P$ to give the protonolysis precursor, **s3**$_P$**·P**. From here, the complex must undergo an internal structural reorganisation involving dissociation of the dative Ca←P interaction to give a slightly less stable **s3**$_{NA}$**·P** (ΔG_L = 23 kJ/mol) conformer. This process is complex, alternative routes have been explored and these will be discussed in greater detail shortly. We believe the overall mechanism will follow this pathway due to a considerably lower

energy associated with a subsequent TS ($\mathbf{TS_{s3NA\bullet P\text{-}s4NA}}$) leading to a substantially stabilised intermediate ($\mathbf{s4_{NA}}$).

$\mathbf{s3_{NA}\bullet P}$ then undergoes proton transfer from $HPPh_2$ to the organophosphine by σ-bond metathesis via $\mathbf{TS_{s3NA\bullet P\text{-}s4NA}}$, the local barrier ΔG_L is a very modest 28 kJ/mol. Decay from $\mathbf{TS_{s3NA\bullet P\text{-}s4NA}}$ leads to the very favourable formation of the organophosphine product and regenerated active catalyst in $\mathbf{s4_{NA}}$, whereby the alkylphosphine is coordinated to the metal centre through a Ca···π interaction involving the original styrene phenyl ring. Dissociation of the organophosphine product, **s5**, from the calcium catalyst is unfavourable, ΔG_L = 35 kJ/mol, consistent with the experimentally observed, much reduced reactivity of styrene compared to vinylpyridine.

In contrast, the vinylpyridine oligomerisation mechanism involves coordination of a second vinylpyridine molecule at $\mathbf{v3_{Ph}}$ to give the oligomerisation precursor $\mathbf{v3_{Ph}\bullet V}$. Unlike the styrene hydrophosphination pathway, dissociation of the Ca···π interaction in $\mathbf{v3_{Ph}\bullet V}$ generates a more favourable intermediate, $\mathbf{v3_{NA}\bullet V}$ (ΔG_L = -26 kJ/mol). Vinylpyridine activation proceeds via the transition state $\mathbf{TS_{v3NA\bullet V\text{-}v4}}$, overcoming a barrier ($\Delta G_L$) of 41 kJ/mol to generate the oligomeric product coordinated to Ca via the N lone pair **v4**.

Regeneration of the active catalyst occurs following a protonolysis step initiated by the coordination of $HPPh_2$ at **v4** to give $\mathbf{v4\bullet P}$. Proton transfer proceeds via $\mathbf{TS_{v4\bullet P\text{-}v5}}$, with a barrier ($\Delta G_L$ = 45 kJ/mol) which is comparable to that associated with a second vinylpyridine insertion step. Decay from $\mathbf{TS_{v4\bullet P\text{-}v5}}$ leads to **v5** whereby the oligomeric phosphine coordinates to the active catalyst through two Ca←N dative interactions.

Formation of **v5** is very favourable (ΔG_L = -114 kJ/mol) and thus dissociation of the oligomer, **v6**, to give the free active catalyst is unfavourable (ΔG_L = 57 kJ/mol relative to **v5**); two weak dative interactions must be broken to release the product.

Overall, for both mechanisms, the considerable thermodynamic stabilities of the products $\mathbf{s4_{NA}}$ (-85 kJ/mol) and **v5** (-176 kJ/mol) provide the necessary driving force to overcome the initial alkene insertion rate limiting step and account for the ready experimental observation of reaction products.

Role of Fluxional Bonding Interactions. The above outlined and simplified mechanism hides significant complexity associated with each individual step and considerable variability in the structural coordination of each species along each reaction pathway. With a perspective of the entire mechanism in place, this detail can now be explored.

The importance of non-covalent interactions in complex organisation has been highlighted previously.[40-42] The most well documented non-covalent bonding motif is the cation···π interaction, involving a strong electrostatic attraction between a positively charged cation and the π electron density of an aromatic system. Cation···π interactions play a fundamental role in biomolecular structure and in materials chemistry.[53-56] The binding energy associated with Ca^{2+}··· η^6-C_6H_6 lies within the range of 290–340 kJ/mol; coordination of an anionic Lewis base at calcium reduces the Ca···π interaction energy to within the region of 130–170 kJ/mol.[42]

Weaker non-covalent interactions such as the Ae···H–X agostic (where X is C or Si) and CH···π interactions are also known to be important for complex structuring. Ae···H–X agostic interaction energies are estimated between 4–40 kJ/mol whereas CH···π interactions have an energy in the range of 6–10 kJ/mol.[40,57] While neither individual interaction has as large an energy as the Ae···π or Ae←dative interactions, both Ae···H–X agostic and CH···π interactions can play a significant role in complex stabilisation due to the formation of multiple interactions having a cumulative stabilising effect.[40]

Consequently, the significance of competing Ca···π and dative Ca←E (E=P or N) interactions as well as weaker structuring Ae···H–X agostic and CH···π interactions are investigated.

Alkene Insertion Precursors. The first step in the hydrophosphination of styrene requires alkene coordination at the Ca complex, $\mathbf{1_{endo}}$. An alternative active catalyst conformer, denoted $\mathbf{1_{exo}}$ was also identified and a detailed examination is found in the ESI, Figure S1.

Upon coordination of styrene at $\mathbf{1_{endo}}$, three conformers were identified, **s2**, $\mathbf{s2_{ene}}$ and $\mathbf{s2_{1,2\_ins}}$ (Figure 3). Styrene can coordinate to Ca via the substituent phenyl ring (Ph_{sty}) to give **s2** (Figure 4a). Formation of **s2**, is enthalpically favourable (ΔH_G = -62 kJ/mol, ESI Table S2) however, the increased ordering within the system renders this association entropically unfavourable ($T\Delta S_G$ = -59 kJ/mol). Nevertheless, coordination of styrene at $\mathbf{1_{endo}}$ remains mildly favourable (ΔG_G = -3 kJ/mol) and is consistent with the experimental observation that coordination of styrene at Ca is a reversible process.[16,17]

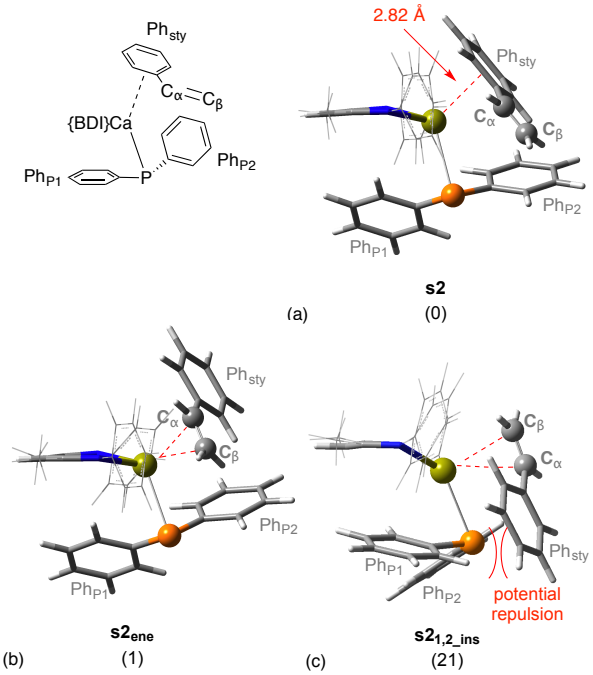

Figure 3. Alkene activation precursors, **s2**, $\mathbf{s2_{ene}}$ and $\mathbf{s2_{1,2\_ins}}$. ΔG_L in kJ/mol in brackets.

QTAIM analysis of **s2** (ESI, Figure S5) identifies numerous bond critical points (BCPs) representing CH···π interactions. A description of QTAIM criteria can be found in the ESI, Computational Methodology. A relatively strong Ca···Ph_{sty} interaction is evident, with an appreciable density at the BCP ρ (0.0123 e/Å^3). The summation of a large number of weak van der Waals (VdW) interactions, as well as the formation of the Ca···Ph_{sty} interaction will contribute to the overall stabilisation of **s2**.[40]

A second coordination mode involving the vinyl moiety (comprising C_α and C_β) is possible; two conformers have been identified differing in phenyl group orientation. **s2**$_{ene}$ (Figure 3b), lies 1 kJ/mol (ESI, Table S6) higher in energy than **s2** whereas **s2**$_{1,2\_ins}$ (Figure 3c) lies 21 kJ/mol higher in energy, possibly as a result of electron repulsion between Ph_{sty} and the phosphorus electron lone pair. These conformers reflect the traditional alkene insertion intermediate observed in analogous intermolecular hydroamination studies. The higher energy associated with **s2**$_{1,2\_ins}$ may be an early indication why 1,2-alkene insertion, associated with the Markovnikov product, is not observed experimentally. Markovnikov vs anti-Markovnikov pathways have been calculated and are discussed later in the manuscript.

The fluxional coordination of styrene at the active catalyst and the small relative free energy difference between these conformers indicates that they are all energetically accessible. However, to limit the number of computations to a manageable number we will continue to follow the lowest (Gibbs free) energy reaction path from **s2**. Additional relevant information related to alkene insertion from **s2**$_{ene}$ can be found in the ESI, Figure S4.

The mechanism for alkene insertion of styrene can be contrasted with that of vinylpyridine. The presence of the lone pair donor N in vinylpyridine and hence formation of a dative bond Ca←N, leads to a single dominant low energy conformer **v2**, Figure 4a. A strong Ca←N dative interaction is identified in the QTAIM analysis of **v2** (ESI, Figure S6), signified by the significant density at the BCP ρ = 0.0324 e/Å^3. A second conformer, analogous to **s2**$_{ene}$ coordinating through the π-system of the vinyl moiety and lacking the Ca←N_{pyr} interaction, has also been identified, **v2**$_{ene}$ (Figure 4b). Comparison of the relative energy of **v2** and **v2**$_{ene}$ indicates that the Ca←N interaction provides approximately ΔG_L = 38 kJ/mol of additional stability.

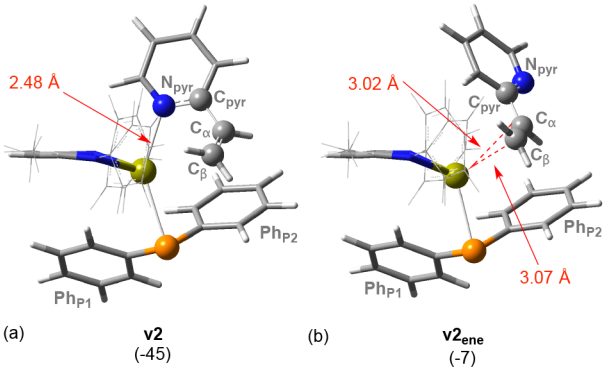

Figure 4. Vinylpyridine activation precursors, **v2** and **v2**$_{ene}$. ΔG_G in kJ/mol in brackets.

Whereas styrene demonstrates weak and fluxional VdW interactions giving rise to numerous coordination modes at the active catalyst, the presence of the lone pair donor N in vinylpyridine leads to a significantly more stable single low energy conformer.

Alkene Insertion Transition States. For styrene, the alkene insertion step proceeds from **s2** via transition state **TS**$_{s2\text{-}s3P}$ (Figure 5a) to intermediate **s3**$_p$. Within **TS**$_{s2\text{-}s3P}$, the arene ring remains weakly coordinated to Ca and the phosphanide moiety is coordinated to Ca via a Ca←P dative interaction.

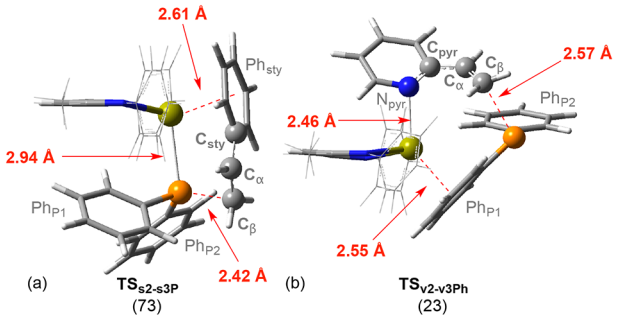

Figure 5. Alkene insertion transition states, **TS**$_{s2\text{-}s3P}$, and **TS**$_{v2\text{-}v3Ph}$. ΔG_G in kJ/mol in brackets.

For vinylpyridine, the alkene insertion step proceeds from **v2** via transition state **TS**$_{v2\text{-}v3Ph}$ (Figure 5b) to intermediate **v3**$_{ph}$. Within **TS**$_{v2\text{-}v3Ph}$, the pyridine ring retains a strong dative interaction and the phosphanide is coordinated to Ca via a pendant Ph group; a Ca···π interaction involving Ph_{P1}. Significantly, there is no Ca←P dative bond, as the Ca←P interaction has increased to 4.15 Å, which is beyond the sum of the constituent ionic radii (3.26 Å). The initiation of bond formation between P-C_β induces a move towards double bond character between C_{sty} and C_α as evidenced by the decreasing bond distance from 1.48 Å in **s2** and **v2** to 1.43 Å in **TS**$_{s2\text{-}s3P}$ and **TS**$_{v2\text{-}v3Ph}$.

Both mechanisms are similar in that there is no interaction of the Ca with the vinyl functionality. The lack of Ca–vinyl bond formation during **TS**$_{s2\text{-}s3P}$ and **TS**$_{v2\text{-}v3Ph}$ is reminiscent of the outer-sphere 1,4-alkene insertion transition state such as that involved in the Eu-catalysed hydrophosphination of 1,3-butadiene.[51] The Ca···π interactions involving Ph_{sty} and Ph_{P1} (in styrene) and N_{pyr} and Ph_{P1} (in vinylpyridine) create pseudo 6-membered and 7-membered ring structures in the transition states as indicated by the presence of BCPs in the QTAIM analysis (ESI, Figure S7). Both transition states, **TS**$_{s2\text{-}s3P}$ and **TS**$_{v2\text{-}v3Ph}$, are significantly more complex than the basic 4-coordinate insertion transition states proposed for hydroamination reactions.[24,50]

The proposition that hydrophosphination is not analogous to hydroamination, but follows a distinct outer sphere mechanism, is a novel aspect of this research. Moreover, the significance of the Ae···π and Ae←donor interactions becomes very clear.

Experimentally, the hydrophosphination of styrene proceeds to give exclusive formation of the anti-Markovnikov product from 2,1-syn addition.[16-19] Barrett *et al.* attributed this observation to the presence the aryl ring at the alkene substrate, which stabilises the accumulation of electron density at C_α during the insertion transition state, lowering the relative energy barrier.[50] We have examined both the anti-Markovnikov (Figure 1) and Markovnikov pathways (ESI, Figure S8), and the relative energy barriers are consistent with this hypothesis.

To investigate the impact of the vinylarene ring during alkene activation in further detail, electron density difference maps (EDDM) were calculated for styrene (**TS**$_{s2\text{-}s3P}$) and vinylpyridine (**TS**$_{v2\text{-}v3Ph}$), Figure 6a and b respectively. Details of the EDDM calculations are found in the ESI, Computational Methodology. The EDDMs illustrate electron density accumulation (red) between Ca and the coordinating species, Ph_{sty} in styrene and N_{pyr} in vinylpyridine, there is also a simultaneous depletion of electron density (blue) around the phosphorus lone pair. Moreover, there is

electron density delocalisation from C_α across the whole ring system in both transition states.

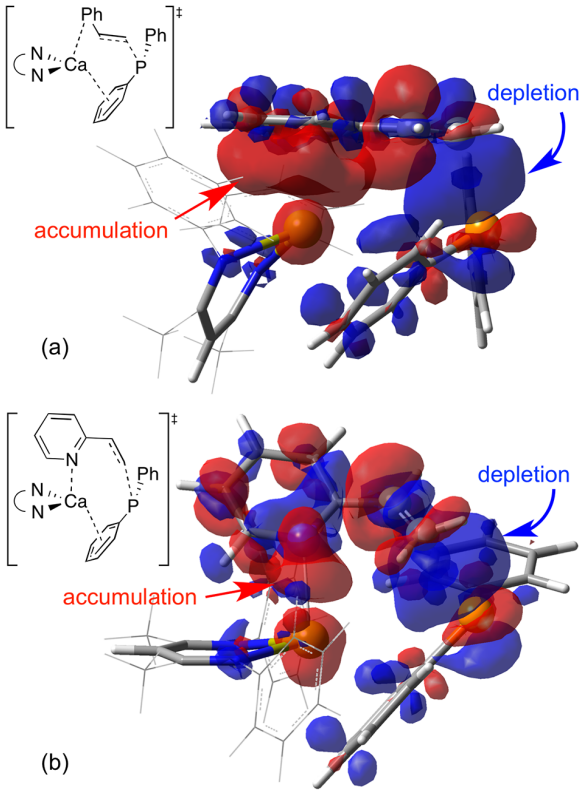

Figure 6. Electron density difference maps for the insertion transition states of styrene (a) and vinylpyridine (b). Isosurfaces (0.004) map areas of electron density accumulation (red) and depletion (blue).

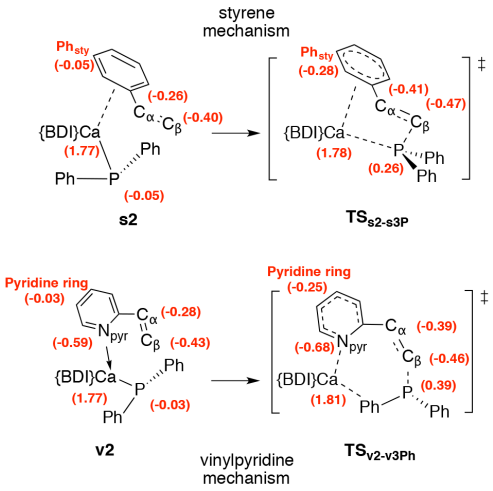

Figure 7. Key NBO charges for **s2**, $\mathbf{TS_{s2\text{-}s3P}}$, **v2** and $\mathbf{TS_{v2\text{-}v3Ph}}$

NBO charge analyses were also performed to investigate the benefit of the vinylarene ring during alkene insertion. The results of the NBO charge analyses for **s2**, $\mathbf{TS_{s2\text{-}s3P}}$, **v2** and $\mathbf{TS_{v2\text{-}v3Ph}}$ are summarised in Figure 7. Moving from alkene insertion precursor to transition state, negative charge accumulates at the C_α position and at the arene ring. The negative charge at Ph_{sty}, in **s2** is -0.05 and increases to -0.28e in $\mathbf{TS_{s2\text{-}s3P}}$. A similar trend is observed for the vinylpyridine complexes, the negative charge at the pyridine ring is -0.03e in **v2** and increases to -0.25e in $\mathbf{TS_{v2\text{-}v3Ph}}$. The increase in negative charge on these rings is concomitant with an increase in positive charge at P, whereas the charge at C_β remains relatively static.

In contrast NBO charge analyses for both the ethene and the Markovnikov insertion pathways (ESI, Figure S9a and b) demonstrate that the lack of an aryl ring leads to a considerably greater negative charge accumulation at C_α in $\mathbf{TS_{e2\text{-}e3Ph}}$ (-0.92e) and C_β in $\mathbf{TS_{1,2\ ins}}$ (-1.02e). Thus, EDDMs and NBO analysis both demonstrate the importance of the aryl ring in reducing the negative charge accumulation at the benzylic C atom and stabilising the activation transition state. Consequently, aryl ring stabilisation accounts in-part for the lower relative energy barriers associated with styrene and vinylpyridine activation (68–73 kJ/mol), compared to the Markovnikov 1,2-addition or ethene insertion mechanisms which have barriers of 100–120 kJ/mol.

Alkene Insertion Products. Decay from transition states $\mathbf{TS_{s2\text{-}s3P}}$ and $\mathbf{TS_{v2\text{-}v3Ph}}$ leads to the products $\mathbf{s3_P}$ and $\mathbf{v3_{Ph}}$ (Figure 8a and b). Similar to $\mathbf{TS_{s2\text{-}s3P}}$, $\mathbf{s3_P}$ maintains a stabilising Ca←P dative and Ca···Ph_{sty} alkylphosphine interaction. Moreover, similar to $\mathbf{TS_{v2\text{-}v3Ph}}$, $\mathbf{v3_{Ph}}$ maintains a strong dative interaction between Ca and the pyridine ring and a phosphanide Ca···π interaction involving Ph_{P1}. In both cases the Ca–vinylarene interaction (styrene Ca···Ph_{sty}, vinypyridine Ca←N) is now stronger and the phosphanide (styrene Ca←P, vinylpyridine Ca···π) interactions are weaker. In both intermediates, the bond distance between C_{sty}–C_α has contracted indicating considerable double bond character.

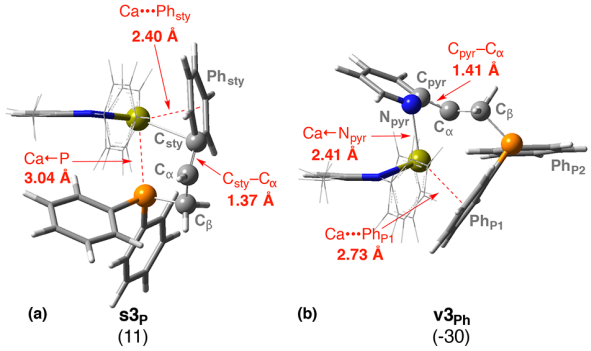

Figure 8. Alkene insertion products, $\mathbf{s3_P}$ and $\mathbf{v3_{Ph}}$, displaying secondary stabilising interactions. ΔG_G in kJ/mol in brackets.

A structural search for alternative conformers allowed **alt_s3P**, to be identified, (ESI, Figure S10). Similar to $\mathbf{s3_P}$, **alt_s3P** replaces the Ca–Ph_{sty} with a Ca–C_α interaction, while the Ca←P interaction is maintained. **alt_s3P** is analogous to the alkene insertion intermediate that would be obtained from a 'traditional' 4-coordinate insertion TS, however the higher energy (+25 kJ/mol relative to $\mathbf{s3_P}$) indicates that coordination through the arene ring (Ca···π) is preferred. In the *β*-diketiminate-stabilised calcium catalysed hydrogenation of 1,1-diphenylethylene, Spielmann *et al.* isolated an important resting state of the cycle in which the vinylarene coordinated to the metal centre via a Ca···π interaction.[58] Computational calculations, conducted by Zeng and Li, found that Ca···π coordination was preferred by 20 kJ/mol relative to an analogous conformer stabilised through an equivalent Ca–C_α interaction.[59] Thus, supporting evidence from the literature confirms that Ca···π coordination can be the preferred interaction mode.

Importantly, in both the styrene and vinylpyridine reaction pathways the 'traditional' alkene coordination is lost and the alkene moiety is instead activated in an outer sphere type mechanism.

Protonolysis Versus Polymerisation. From the alkene insertion intermediates **s3$_P$** and **v3$_{Ph}$** the styrene and vinylpyridine reaction pathways can proceed in one of two directions, polymerisation involving a second alkene insertion step to generate a polymeric(oligomeric) product, or protonolysis terminating the reaction and generating an organophosphine product. It has been experimentally established that the outcome is dependent on the alkene, thus we now investigate both mechanisms to understand why protonolysis is the favoured outcome for styrene and polymerisation is the favoured outcome for vinylpyridine.

Styrene: Protonolysis Pathway. Coordination of $HPPh_2$ in the vacant axial site at **s3$_P$** to give **s3$_P$•P** (ESI, Figure S11) is a strongly enthalpically favoured process (ΔH_L = -72 kJ/mol) as a consequence of the formation of the Ca←P' dative interaction. However, the strong association leads to increased structuring and the formation of **s3$_P$•P** is only moderately favourable, ΔG_L = -22 kJ/mol.

The alkylphosphine substrate can coordinate via a Ca←P dative interaction or via a Ca···π interaction involving one of the phenyl groups. These interactions are competitive, as Ca···π interactions are known to exhibit comparable energies to dative interactions.[40-42] Moreover, we have shown here that the alkylphosphine moiety can coordinate interchangeably between these modes (Ca←P and Ca···π). Energy profiles corresponding to a rotation about the C_β–P bond leading to substitution of the Ca←P for a Ca···π (Ph_{P1}) (blue) interaction, as well as a rotation about the C_α–C_β bond leading to deactivation of the Ca←P interaction (red) are presented in Figure 9. Details of the computational procedure can be found in the ESI, Computational Methodology.

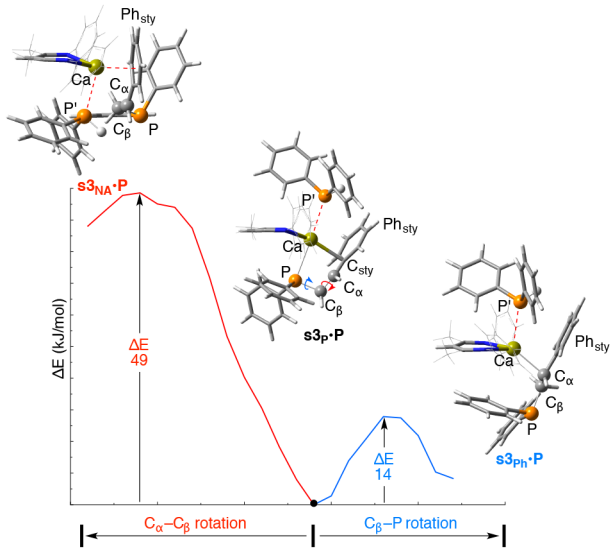

Figure 9. Rotational energy profile corresponding to C_α–C_β (red) and C_β–P (blue) bond rotations. ΔE in kJ/mol.

Starting from **s3$_P$•P** rotation about the C_α–C_β bond produces **s3$_{NA}$•P** (Figure 9, red line), whereby the Ca←P dative bond has been deactivated and coordination of the alkylphosphine now occurs exclusively via a Ca···π interaction through Ph_{sty} (2.38 Å). We estimate the ΔG rotational barrier to be ≈59 kJ/mol, where we have assumed TΔΔS is -10 kJ/mol, based on the marginal general increase of TΔS computed for other transition states examined in this study.

Starting from **s3$_P$•P**, rotation about the C_β–P bond produces **s3$_{Ph}$•P**, (Figure 9, blue line) whereby the alkylphosphine Ca←P dative bond is substituted for a Ca···π (Ph_{P1}) interaction. During this process the alkylphosphine fragment exchanges the Ca···C_{sty} for a Ca–C_α interaction, maintaining a pseudo-5 membered ring involving Ca–C_α–C_β–P–Ph_{P1}. The rotational energy barrier ΔE = 14 kJ/mol. Moreover, despite the structural reorganisation on moving from **s3$_P$•P** to **s3$_{Ph}$•P**, there is a negligible difference in enthalpy (ΔH_L = 3 kJ/mol) and free energy (ΔG_L = 6 kJ/mol) between these conformers.

Crucially, the relative energy barriers associated with the interconversion from **s3$_P$•P** to **s3$_{Ph}$•P** or **s3$_{NA}$•P** are less than the local relative enthalpy associated with styrene insertion (ΔH_L = 70 kJ/mol), which would suggest that all of these intermediates are easily accessible under experimental conditions. Moreover, all three lie within an energy range of approximately 20 kJ/mol, suggesting that protonolysis is feasible from all three intermediates. Consequently, protonolysis has been explored (Figure 10) from each conformer; **s3$_P$•P** (black), **s3$_{Ph}$•P** (blue) and **s3$_{NA}$•P** (red). Relative ΔH, TΔS and ΔG are presented in the ESI, Table S7.

Protonolysis proceeds via the transition states **TS$_{s3P•P-s4P}$**, **TS$_{s3Ph•P-s4Ph}$** and **TS$_{s3NA•P-s4NA}$**, (Figure 10) involving H migration from $HPPh_2$ to the alkylphosphine fragment. In **TS$_{s3P•P-s4P}$** and **TS$_{s3Ph•P-s4Ph}$** non-covalent interactions are maintained, leading to sterically congested structures, which consequently have considerable Gibbs free energy barriers (85 kJ/mol). In comparison, **TS$_{s3NA•P-s4NA}$**, has no Ca←P interaction, reduced congestion and a much lower Gibbs free energy barrier (40 kJ/mol).

Although the intermediate **s3$_P$•P** corresponds to the most stable protonolysis precursor, the corresponding transition state, **TS$_{s3P•P-s4P}$**, is thermodynamically unfavourable, (ΔG_L = 96 kJ/mol), and thus is kinetically retarded. The **s3$_{Ph}$•P** conformer and associated **TS$_{s3Ph•P-s4Ph}$** are essentially degenerate with **s3$_P$•P** pathway, and thus, protonolysis is also kinetically unfavourable.

In contrast, **s3$_{NA}$•P** is destabilised relative to **s3$_P$•P** (ΔG_L = 22 kJ/mol) and a higher rotational barrier (ΔG ≈ 59 kJ/mol) must be overcome to form **s3$_{NA}$•P**. While higher in energy, this rotational barrier is still experimentally accessible. Importantly, the barrier (ΔG_L = 29 kJ/mol) to protonolysis at **s3$_{NA}$•P** is significantly lower than for the other conformers **s3$_P$•P** and **s3$_{Ph}$•P**. Thus it is anticipated that protonolysis will proceed via the kinetically more favourable two-step pathway involving the interconversion of **s3$_P$•P** to **s3$_{NA}$•P** and then the thermodynamically more favourable transition state, **TS$_{s3NA•P-s4NA}$**.

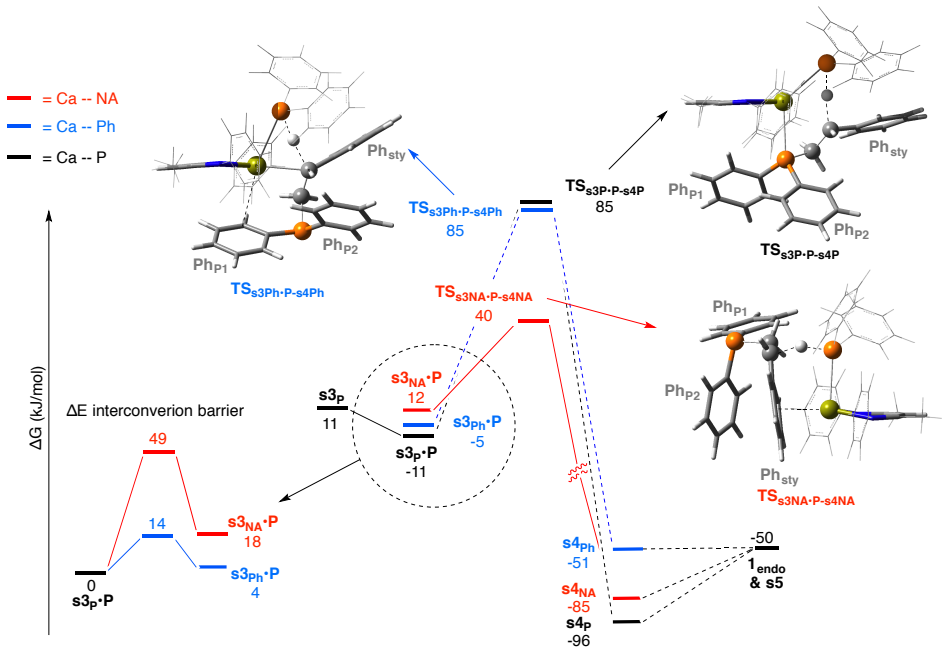

Figure 10. The relative energy profile for styrene protonolysis. ΔG_G and ΔG_L in kJ/mol. Inset represents the energy barrier (ΔE in kJ/mol) for the interconversion of protonolysis precursor intermediates.

Proton transfer generates very stable (ΔG = -51 – -96 kJ/mol) product-coordinated conformers **s4**$_P$, **s4**$_{Ph}$ and **s4**$_{NA}$ (ESI, Figure S12) which provide the thermodynamic driving force for the reaction. In **s4**$_P$ the organophosphine product coordinates to the regenerated active catalyst through the Ca←P dative interaction (3.01 Å). In **s4**$_{Ph}$, the distance between Ca and Ph$_{P1}$ increases to 5.23 Å, and the product coordinates via numerous Ca···π interactions. In **s4**$_{NA}$ the product coordinates via a Ca···π interaction involving Ph$_{sty}$ (2.75 Å).

Dissociation of the organophosphine product, **s5**, from **s4**$_{NA}$ and **s4**$_P$ to give the regenerated active catalyst **1**$_{endo}$ is unfavourable (ΔG_L= 35 – 46 kJ/mol). Conversely, dissociation of the organophosphine product from **s4**$_{Ph}$ is a facile process due to the negligible difference in energies.

The overall stability of **s4**$_P$ and **s4**$_{NA}$, indicate that these Ca-product conformers correspond to the resting state(s) for the hydrophosphination mechanism and indicate that product inhibition may occur at high concentrations of alkylphosphine. The Hill group did not report having observed any product inhibition for the calcium-catalysed hydrophosphination, however product inhibition has been observed by the Marks' group while exploring lanthanide-catalysed intramolecular hydrophosphination.[16,60]

Styrene: Oligomerisation Pathway. Oligomerisation involving a second styrene molecule has been investigated and is compared to the protonolysis pathway in Figure 11. Relative ΔH, $T\Delta S$ and ΔG values are presented in the ESI, Table S8.

Substituting HPPh$_2$ in **s3**$_{NA}$**•P** with styrene results in **s3**$_{NA}$**•S** (ESI, Figure S13a), where coordination is through a Ca···π interaction via the vinyl moiety of styrene. Styrene insertion proceeds via **TS**$_{s3NA\cdot S\text{-}s4poly}$ (Figure 11), whereby the mechanism involves the formation of a Ca–C$_\alpha$ bond rather than a Ca···Ph$_{sty}$ interaction as observed in the first styrene insertion step. **TS**$_{s3NA\cdot S\text{-}s4poly}$ has a larger global energy than the first styrene insertion transition state. However, this second insertion step proceeds from a higher energy intermediate and the local barrier to insertion is actually lower by 31 kJ/mol. Nevertheless, the higher global barrier to oligomerisation indicates why polymerisation is not observed experimentally for styrene.

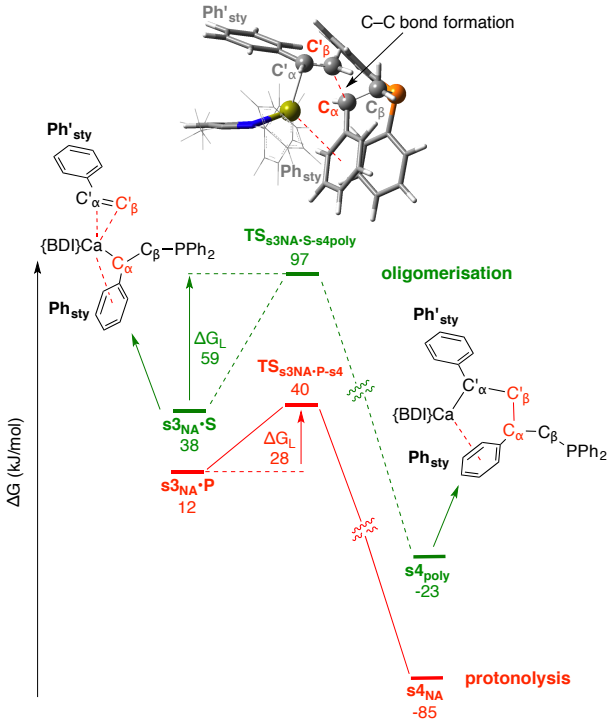

Figure 11. The relative energy profile for styrene oligomerisation from **s3**$_{NA}$**•S** (green) and protonolysis from **s3**$_{NA}$**•P** (red). ΔG_G and ΔG_L in kJ/mol.

Decay from **TS**$_{s3NA\cdot S\text{-}s4poly}$ leads to intermediate **s4**$_{poly}$ (ESI, Figure S13b), consisting of the oligomeric product coordinated to the metal centre through Ca–C$_\alpha$ and Ca···π interactions. Formation of

s4$_{poly}$ is favourable relative to the intermediates involved in the oligomerisation mechanism, however it is significantly less favourable than the protonolysis products. Thus, compared to protonolysis, not only is the barrier to oligomerisation considerably higher, the products are significantly less stable.

Moreover, **TS**$_{s3NA\cdot S\text{-}s4poly}$ is of comparable energy to the high-energy protonolysis transition states, **TS**$_{s3P\cdot P\text{-}s4P}$ and **TS**$_{s3Ph\cdot P\text{-}s4Ph\cdot}$ Thus, if oligomerisation is not observed experimentally, we cannot expect the protonolysis transition states to be accessible, consequently, this observation lends greater weight to the hypothesis that the 'NA' protonolysis pathway is dominant.

Vinylpyridine: Protonolysis & Oligomerisation. Attention is now turned toward exploring the protonolysis and oligomerisation pathways for vinylpyridine. The relative energy profile for both pathways is provided in Figure 12, ΔH, TΔS and ΔG are presented in the ESI, Tables S9 and S10.

Addition of vinylpyridine to **v3**$_{Ph}$, generates the oligomerisation precursor, **v3**$_{Ph}$**•V** (ESI, Figure S14a). Coordination is via a Ca←N dative interaction and is enthalpically favourable (ΔH_L = -63 kJ/mol), moreover the Ca···π interaction with Ph_{P1} is maintained. However, increased ordering within the system ($T\Delta S_L$ = -54 kJ/mol) means formation of **v3**$_{Ph}$**•V** is only just favourable (ΔG_L = -9 kJ/mol).

In analogy with styrene, two alternative conformers have been located, one with the alkylphosphine exhibiting a secondary Ca←P interaction, **v3**$_{P}$**•V** (ESI, Figure S14b) and one with the Ca←P interaction switched off (the alkylphosphine coordinating only via a Ca···π interaction), **v3**$_{NA}$**•V** (ESI, Figure S14c). Both **v3**$_{Ph}$**•V** and **v3**$_{P}$**•V** lie higher in energy than **v3**$_{NA}$**•V** (ΔG_L = 30 and 25 kJ/mol respectively) due to increased steric crowding. Thus we have only probed the oligomerisation mechanism from the lowest energy oligomerisation precursor, **v3**$_{NA}$**•V**.

Vinylpyridine activation proceeds through the transition state **TS**$_{v3NA\cdot V\text{-}v4}$ (Figure 12), with a modest local free energy barrier (ΔG_L = 41 kJ/mol). Formation of the Ca-coordinated organophosphine oligomer in **v4** (ESI, Figure S15) is favourable (ΔG_G = -115 kJ/mol) providing the thermodynamic driving force for the reaction. The newly formed organophosphine coordinates to Ca via two Ca←N interactions. Nevertheless **v4** is not significantly more stable than the analogous **s4** (+30 kJ/mol), Figure 1.

Substituting the second vinylpyridine molecule in **v3**$_{NA}$**•V** for $HPPh_2$ results in **v3**$_{NA}$**•P** (ESI, Figure S16a). Both molecules have similar free energies as one dative interaction (Ca←N) has simply been replaced with another (Ca←P). Protonolysis pathways from **v3**$_{NA}$**•P** and **v3**$_{NA}$**•V** are compared in Figure 12. Protonolysis at **v3**$_{NA}$**•P** proceeds through transition state **TS**$_{v3NA\cdot P\text{-}v4prot}$, the local free energy barrier is 65 kJ/mol, whereas that for oligomerisation is only ΔG_L = 41 kJ/mol. Thus, the protonolysis barrier is significantly higher in energy (by 34 kJ/mol), offering clear evidence for why, in stark contrast to styrene, polymerisation is favoured over protonolysis when vinylpyridine is used as the substrate in experiments.[16] The protonolysis product, **v4**$_{prot}$ (ESI, Figure S16b), consists of the organophosphine product coordinated to the regenerated active catalyst through a dative Ca←N bond. Similar to **v4**, formation of **v4**$_{prot}$ is thermodynamically very favourable (ΔG_G = -120 kJ/mol).

To ensure regeneration of the active catalyst from **v4** was not rate limiting, oligomerisation termination via protonolysis has been examined and is contrasted with a third vinylpyridine insertion step (see ESI, Oligomerisation Termination and Third Vinylpyridine Insertion). The barrier to oligomerisation termination via protonolysis was ΔG_L = 44 kJ/mol whereas the third insertion step has a barrier of ΔG_L = 48 kJ/mol. Neither pathway can be considered as rate limiting as the initial alkene insertion step barrier is ΔG_L = 68 kJ/mol.

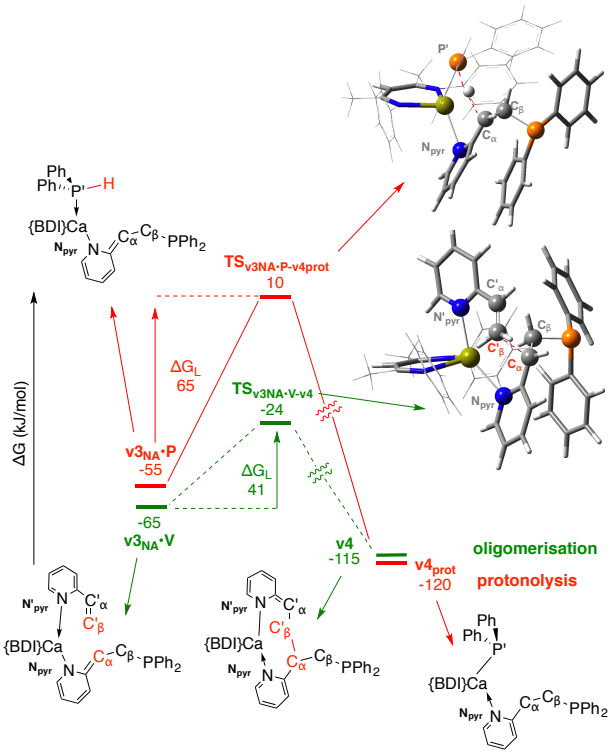

Figure 12. The relative energy profile for vinylpyridine oligomerisation from **v3**$_{NA}$**•V** (green) and protonolysis from **v3**$_{NA}$**•P** (red). ΔG_G and ΔG_L in kJ/mol.

Comparison of Mechanistic Pathways. Having outlined the styrene and vinylpyridine reaction mechanisms in detail, we now return to the overall reaction summarised in Figure 1 and make a comparison of the favoured pathways.

The largest local free energy barrier (ΔG_L) for both reactions corresponds to the first step in the catalytic cycle, alkene insertion of the substrate. Moreover, both barriers are similar, styrene insertion ΔG_L =76 kJ/mol and vinylpyridine ΔG_L=68 kJ/mol..

Our computed barrier to styrene insertion is supported by experimentally derived values calculated from Eyring analysis.[17] Liu *et al.* who employed a related calcium catalyst experimentally determined the enthalpy (ΔH) and free energy (ΔG) of styrene hydrophosphination was 68 (± 5) kJ/mol and 98 (± 10) kJ/mol respectively. Our calculations indicate that for the same step the local enthalpy (ΔH_L) and free energy (ΔG_L) barriers are 70 kJ/mol and 76 kJ/mol respectively. Although there is a larger difference between the ΔG values (22 kJ/mol), reminiscent of the difficulties in computing accurate ΔS values, good agreement is observed between the experimental and computed ΔH (2 kJ/mol).

The similar alkene insertion energy barriers do not immediately indicate why, experimentally, the vinylpyridine reaction proceeds under more favourable conditions than the styrene mechanism.[16] However, we have shown that the relevant intermediates and

transition states of the vinylpyridine pathway have lower global energy values, principally due to the stronger Ca←N dative interaction of vinylpyridine relative to the Ca···π interactions observed for styrene (ESI, Table S12). Moreover, the combined local Gibbs free energy barriers along the styrene pathway are higher 76+59+28=166 kJ/mol compared to those for vinylpyridine 68+41=109 kJ/mol.

The facility of the vinylpyridine reaction also likely lies, in part, in the relative energy differences of the alkene insertion precursors **s2** and **v2**. Coordination of styrene at the active catalyst, $\mathbf{1}_{\mathbf{endo}}$ to give **s2** is facile (ΔG_L = -3 kJ/mol). This will be more difficult at a more sterically crowded Ca centre. Experimental conditions are likely to include fluxional coordination of solvent, product and THF molecules, thus requiring more forcing reaction conditions to promote dissociation of these substrates. In contrast, **v2** forms a favourable Ca←N dative interaction that is significantly more favourable (ΔG_L = -45 kJ/mol) and thus less likely to be displaced once formed, allowing the reaction to proceed.

The globally lower energy pathway, reduced overall Gibbs free energy barriers, and the coordinative stability of the alkene insertion precursor therefore combine to provide a rationalisation for the facilitated reactivity of vinylpyridine compared to styrene.

For styrene, the protonolysis barrier is significantly more favourable (ΔG_L = 28 kJ/mol, Figure 11) than the oligomerisation barrier (ΔG_L = 59 kJ/mol, Figure 11). Conversely, in the vinylpyridine mechanism the (first) protonolysis barrier is significantly less favourable (ΔG_L = 65 kJ/mol, Figure 12) than the second insertion barrier (ΔG_L = 41 kJ/mol, Figure 12). In both cases, our calculations are supported by the experimentally observed outcomes.[16]

For both the styrene and vinylpyridine reaction mechanisms the protonolysis products, **s4** and **v5**, correspond to the resting state of the reaction. **s4** has ΔG_G = -85 kJ/mol whereas **v5** is substantially stabilised, ΔG_G = -176 kJ/mol. In the vinylpyridine energy profile, the stability of **v5** would indicate a likelihood of significant product inhibition, particularly as dissociation of the oligomeric product from the Ca centre is energy intensive (ΔG_L = 57 kJ/mol). However, the stability of **v5** may be enhanced in the model system as a consequence of reduced steric hindrance, under experimental conditions, the favourable coordination of the oligomer at the active catalyst may be reduced.

CONCLUSIONS

The aim of this computational investigation has been to explore the competing mechanisms by which calcium catalysed hydrophosphination and polymerisation occur. A key feature of this investigation has been the importance of non-covalent interactions Ca···π, CH···π, Ca···H–X which clearly have the potential to play a very significant role once sterically demanding ligands and vinylarene activated substrates are employed as part of the computational model. One goal has been to establish if, as hypothesised, the hydrophosphination mechanism is analogous to Ca-catalysed hydroamination. A second goal has been to rationalise why hydrophosphination is favoured for styrene and polymerisation is favoured for vinylpyridine.

An important insight provided by this work, is that the hydrophosphination reaction mechanism is more complex and quite distinct from the hydroamination reaction. This is made clear in the first step, where coordination of the unsaturated substrate at the metal centre is not via the vinyl moiety. Styrene coordinates preferentially through a Ca···π interaction involving the arene ring, and vinylpyridine coordinates preferentially via a Ca←N dative interaction. Alkene insertion proceeds via an outer sphere conjugative addition mechanism, where there is no direct interaction of Ca with the vinyl functionality. Ca···π interactions involving Ph_{sty} and Ph_{P1} (in styrene) and N_{pyr} and Ph_{P1} (in vinylpyridine) create pseudo 6-membered and 7-membered ring structures in their respective the transition states. This is in contrast to the intermolecular hydroamination reaction in which the alkylamine product is stabilised at Ca exclusively through a secondary Ca←N dative interaction, which is maintained throughout protonolysis.[24,50] In both cases, this contradicts earlier mechanisms based upon experimental observations.[16,52]

We have established that hydrophosphination is favoured for styrene and oligomerisation is favoured for vinylpyridine. The computed mechanism is consistent with the experimentally based hypothesis that a second vinylpyridine insertion step is kinetically more favourable than protonolysis). However, termination protonolysis of the nacent oligomer, has a barrier competitive with the on-going polymerisation. It is probable that the preference for polymerisation is in-part dependent on the stability of Ca←N interaction with vinylpyridine which dominates the weaker Ca←P interaction of $HPPh_2$. The corollary however, is that in the absence of other coordinating ligands, the stability of the coordinated oligomeric product is significant and constitutes the resting state for this mechanism.

In particular, our research has shown the significance of BDI-substrate CH···π, Ca···π and Ca←donor interactions, which play a critical role in both the hydrophosphination and oligomerisation mechanisms. Ca···π interactions include those with the Ph groups of PPh_2H and styrene. The significance of such interactions is easily overlooked as a consequence of model simplification, a focus only on inner sphere coordination mechanisms and/or a reduced ability to adequately recover dispersion interactions.

Ca···π and Ca←donor interactions tether the alkylphosphine or styrene to the Ca centre. We have also found that the fluxional interchange between the Ca···π and Ca←donor interactions means that numerous conformers are possible, leading to various protonolysis (and oligomerisation) pathways. The kinetically most favourable pathway for styrene protonolysis and vinylpyridine oligomerisation proceed from the least sterically hindered conformers which exhibit no stabilisation through the P terminus of the alkylphosphine substrate.

COMPUTATIONAL METHODOLOGY

Full details of the computational methodology can be found in the ESI.

AUTHOR INFORMATION

Corresponding Authors

* Email for B.J.W.: b.ward11@imperial.ac.uk
* Email for P.A.H.: p.hunt@imperial.ac.uk.

Notes

The authors declare no competing financial interest.

ASSOCIATED CONTENT

Supporting Information

Supporting Information Available: Geometric parameters of intermediates and transition states; QTAIM and NBO charges of selected intermediates and transition states; Representation of the structures of intermediates not reported in the text (PDF) Cartesian coordinates of all the reaction intermediates and transition states (PDF). This material is available free of charge via the Internet at http://pubs.acs.org.

ACKNOWLEDGMENT

The authors wish to acknowledge the EPSRC (EP/1014853/1) for studentship funding for Bryan J. Ward. The authors thank Dr Richard Matthews for his assistance with the generation of EDDMs.

REFERENCES

(1) Koshti, V.; Gaikwad, S.; Chikkali, S. H. *Coord. Chem. Rev.* **2014**, *265*, 52-73.
(2) Harder, S. *Chem Rev* **2010**, *110*, 3852-3876.
(3) Reznichenko, A. L.; Hultzsch, K. C. In *Molecular Catalysis of Rare-Earth Elements*; Roesky, P. W., Ed. 2010; Vol. 137, pp 1-48.
(4) Alonso, F.; Moglie, Y.; Radivoy, G.; Yus, M. *Green Chem.* **2012**, *14*, 2699-2702.
(5) Del Sesto, R. E.; Corley, C.; Robertson, A.; Wilkes, J. S. *J. Organomet. Chem.* **2005**, *690*, 2536-2542.
(6) McNulty, J.; Nair, J. J.; Cheekoori, S.; Larichev, V.; Capretta, A.; Robertson, A. J. *Chem. Eur. J.* **2006**, *12*, 9314-9322.
(7) Tsunashima, K.; Niwa, E.; Kodama, S.; Sugiya, M.; Ono, Y. *The J. Phys. Chem. B* **2009**, *113*, 15870-15874.
(8) Armel, V.; Velayutham, D.; Sun, J.; Howlett, P. C.; Forsyth, M.; MacFarlane, D. R.; Pringle, J. M. *J. Mater. Chem.* **2011**, *21*, 7640-7650.
(9) Rana, U. A.; Vijayaraghavan, R.; Walther, M.; Sun, J.; Torriero, A. A. J.; Forsyth, M.; MacFarlane, D. R. *Chem. Commun.* **2011**, *47*, 11612-11614.
(10) Scarbath-Evers, L. K.; Hunt, P. A.; Kirchner, B.; MacFarlane, D. R.; Zahn, S. *PCCP* **2015**, *17*, 20205-20216.
(11) Ramnial, T.; Ino, D. D.; Clyburne, J. A. C. *Chem. Comm.* **2005**, 325-327.
(12) Fraser, K. J.; MacFarlane, D. R. *Aust. J. Chem.* **2009**, *62*, 309-321.
(13) Zhang, Y.; Zhang, S.; Lu, X.; Zhou, Q.; Fan, W.; Zhang, X. *Chem. Eur. J.* **2009**, *15*, 3003-3011.
(14) O'Toole, G. A.; Wathier, M.; Zegans, M. E.; Shanks, R. M. Q.; Kowalski, R.; Grinstaff, M. W. *Cornea* **2012**, *31*, 810-816.
(15) Choi, S. Y.; Rodriguez, H.; Mirjafari, A.; Gilpin, D. F.; McGrath, S.; Malcolm, K. R.; Tunney, M. M.; Rogers, R. D.; McNally, T. *Green Chem.* **2011**, *13*, 1527-1535.
(16) Crimmin, M. R.; Barrett, A. G. M.; Hill, M. S.; Hitchcock, P. B.; Procopiou, P. A. *Organometallics* **2007**, *26*, 2953-2956.
(17) Liu, B.; Roisnel, T.; Carpentier, J.-F.; Sarazin, Y. *Chem. Eur. J.* **2013**, *19*, 13445-13462.
(18) Hu, H.; Cui, C. *Organometallics* **2012**, *31*, 1208-1211.
(19) Anga, S.; Carpentier, J.-F.; Panda, T. K.; Roisnel, T.; Sarazin, Y. *RSC Adv.* **2016**, *6*, 57835-57843.
(20) Hill, M. S.; Liptrot, D. J.; Weetman, C. *Chem. Soc. Rev.* **2016**, *45*, 972-988.
(21) Al-Shboul, T. M. A.; Goerls, H.; Westerhausen, M. *Inorg. Chem. Comm.* **2008**, *11*, 1419-1421.
(22) Hu, H. F.; Cui, C. M. *Organometallics* **2012**, *31*, 1208-1211.
(23) Bange, C. A.; Waterman, R. *Chem. Eur. J.* **2016**, 22, 12598–12605.
(24) Tobisch, S. *Chem. Eur. J.* **2014**, 20, 8988-9001.
(25) Tobisch, S. *Chem. Eur. J.* **2011**, 17, 14974-14986.
(26) Tobisch, S. *Chem. Eur. J.* **2015**, 21, 6765-6779.
(27) Zhang, X.; Tobisch, S.; Hultzsch, K. C. *Chem. Eur. J.* **2015**, *21*, 7841-7857.
(28) NBO, version 5.9; Glendening, E. D.; Badenhoop, J, K.; Reed, A. E.; Carpenter, J. E.; Bohmann, J. A.; Morales, C. M.; Weinhold, F. Theoretical Chemistry Institute, University of Wisconsin, Madison, 2001.
(29) AIMAll, version 14.11.23, Keith, T. A. TK Gristmill Software, Overland Park KS, USA, 2014.
(30) Prates Ramalho, J. P.; Gomes, J. R. B.; Illas, F. *RSC Adv.* **2013**, *3*, 13085-13100.
(31) Matthews, R. P.; Welton, T.; Hunt, P. A. *PCCP* **2014**, *16*, 3238-3253.
(32) Savarese, M.; Brémond, É.; Adamo, C. *Theor. Chem. Acc.* **2016**, *135*, 1-11.
(33) Peverati, R.; Truhlar, D. G. Quest for a universal density functional: the accuracy of density functionals across a broad spectrum of databases in chemistry and physics, 2014; Vol. 372.
(34) Goerigk, L.; Grimme, S. *PCCP* **2011**, *13*, 6670-6688.
(35) Thanthiriwatte, K. S.; Hohenstein, E. G.; Burns, L. A.; Sherrill, C. D. *J. Chem. Theor. Comp.* **2011**, *7*, 88-96.
(36) Minenkov, Y.; Singstad, A.; Occhipinti, G.; Jensen, V. R. *Dalton Trans.* **2012**, *41*, 5526-5541.
(37) Li, A.; Muddana, H. S.; Gilson, M. K. *J. Chem. Theor. Comp.* **2014**, 10, 1563-1575.
(38) Barrett, A. G. M.; Crimmin, M. R.; Hill, M. S.; Procopiou, P. A. *Proc. R. Soc. A* **2010**, 466, 927-963.
(39) Ruspic, C.; Harder, S. *Inorg. Chem.* **2007**, *46*, 10426-10433.
(40) Buchanan, W. D.; Allis, D. G.; Ruhlandt-Senge, K. *Chem. Comm.* **2010**, *46*, 4449-4465.
(41) Torvisco, A.; O'Brien, A. Y.; Ruhlandt-Senge, K. *Coord. Chem. Rev.* **2011**, *255*, 1268-1292.
(42) Loh, C.; Seupel, S.; Goerls, H.; Krieck, S.; Westerhausen, M. *Organometallics* **2014**, *33*, 1480-1491.
(43) Torvisco, A.; Decker, K.; Uhlig, F.; Ruhlandt-Senge, K. *Inorg. Chem.* **2009**, *48*, 11459-11465.
(44) Tomasi, J. *Theor. Chem. Acc.* **2004**, *112*, 184-203.
(45) Kozuch, S.; Shaik, S. *Acc. Chem. Res.* **2011**, *44*, 101-110.
(46) Ribeiro, R. F.; Marenich, A. V.; Cramer, C. J.; Truhlar, D. G. *J. Phys. Chem. B* **2011**, *115*, 14556-14562.
(47) Ayala, P. Y.; Schlegel, H. B. *J. Chem. Phys.* **1998**, *108*, 2314-2325.
(48) Ardura, D.; López, R.; Sordo, T. L. *J. Phys. Chem. B* **2005**, *109*, 23618-23623.
(49) Leung, B. O.; Reid, D. L.; Armstrong, D. A.; Rauk, A. *J. Phys. Chem. A* **2004**, *108*, 2720-2725.
(50) Barrett, A. G.; Brinkmann, C.; Crimmin, M. R.; Hill, M. S.; Hunt, P.; Procopiou, P. A. *J. Am. Chem. Soc.* **2009**, *131*, 12906-12907.
(51) Mercy, M.; Maron, L. *Dalton Trans* **2009**, 3014-3025.
(53) Liu, B.; Roisnel, T.; Carpentier, J.-F.; Sarazin, Y. *Chem. Eur. J.* **2013**, *19*, 2784-2802.
(53) Dougherty, D.; Stauffer, D. *Science* **1990**, *250*, 1558-1560.
(54) Gallivan, J. P.; Dougherty, D. A. *Proc. R. Soc.* **1999**, 96, 9459-9464.
(55) Masson, E.; Schlosser, M. *Org. Lett.* **2005**, *7*, 1923-1925.
(56) Rooman, M.; Liévin, J.; Buisine, E.; Wintjens, R. *J. Mol. Bio.* **2002**, *319*, 67-76.
(57) Scherer, W.; McGrady, G. S. *Angew. Chem. Int. Ed.* **2004**, *43*, 1782-1806.
(58) Spielmann, J.; Buch, F.; Harder, S. *Angew. Chem. Int. Ed.* **2008**, 47, 9434-9438.
(59) Zeng, G.; Li, S. *Inorg. Chem.* **2010**, *49*, 3361-3369.
(60) Douglass, M. R.; Stern, C. L.; Marks, T. J. *J. Am. Chem. Soc.* **2001**, *123*, 10221-10238.

Authors are required to submit a graphic entry for the Table of Contents (TOC) that, in conjunction with the manuscript title, should give the reader a representative idea of one of the following: A key structure, reaction, equation, concept, or theorem, etc., that is discussed in the manuscript. Consult the journal's Instructions for Authors for TOC graphic specifications.